Solar Physics (2025) 300:80
https://doi.org/10.1007/s11207-025-02490-4

RESEARCH

Revisiting the Winding Angle of the Heliospheric Magnetic Field: Investigating the Influence of Turbulence

F.H. van der Merwe[1] · **N.E. Engelbrecht**[1,2]

Received: 14 November 2024 / Accepted: 17 May 2025
© The Author(s) 2025

Abstract
The nature, and geometry, of the heliospheric magnetic field (HMF) plays a significant role in the transport of energetic charged particles, whether these be of solar or galactic origin. The present study investigates the winding angle of the HMF by analysing almost 60 years of spacecraft data, by employing methods based on the assumption of a Parker HMF from prior studies, as well as a 3D definition of the winding angle. The 2D results reveal an overwound (relative to the expected Parker field result) winding angle with a clear solar cycle dependence, in agreement with previous studies. The 3D results, however, indicate a consistently underwound field. It is further demonstrated that this winding can potentially be explained by the meandering of HMF lines due to the presence of turbulence. Furthermore, consequences of this phenomenon for energetic particle transport, particularly for magnetic focusing, are discussed.

Keywords Magnetic fields, interplanetary · Solar cycle, observations · Turbulence · Energetic particles, propagation

1. Introduction

An understanding of the nature, and geometry, of the heliospheric magnetic field (HMF) is essential to our understanding not only of the Sun and its dynamical plasma environment, but also plays a significant role in the transport of energetic charged particles such as solar energetic particles and galactic cosmic rays (see, e.g., Engelbrecht et al. 2022, and references therein). The geometry of the HMF is particularly important, as this governs whether diffusion parallel to the HMF dominates the transport of these particles, or the significantly less-effective diffusion perpendicular to this field, with direct consequences for the Earth's radiation environment. As humanity expands its activities in space, then, it is increasingly

✉ F.H. van der Merwe
frans.h.vandermerwe@gmail.com

N.E. Engelbrecht
n.eugene.engelbrecht@gmail.com

1 Centre for Space Research, North-West University, 2520, Potchefstroom, South Africa

2 National Institute for Theoretical and Computational Sciences (NITheCS), Stellenbosch, South Africa

Published online: 06 June 2025

imperative that the radiation risks (see, e.g., Schwadron et al. 2014; Barthel and Sarigul-Klijn 2019; Slaba 2021; Guo et al. 2021) inherent to these endeavours be ameliorated in some way. One potential way to do so would be to provide simulation-based early-warning systems (see, e.g., Posner et al. 2013; Engell et al. 2017; Posner and Strauss 2020; Whitman et al. 2023). For early warning systems pertaining to Mars-bound missions, early solar energetic particle (SEP) event warning systems would rely on the Hohmann-Parker effect, where often the Earth and a spacecraft on a Hohmann transfer trajectory[1] have been demonstrated by Posner et al. (2013) to be magnetically well-connected via a Parker (1958) spiral HMF line. These authors, however, considered only the magnetic connection between Earth and a spacecraft on a Hohmann transit for the case of a nominal Parker spiral field (more on this below), and did not take into account natural variations in the HMF geometry that could arise from the turbulent meandering of HMF lines (see, e.g., Matthaeus et al. 1995; Ruffolo, Chuychai, and Matthaeus 2006; Ragot 2011; Shalchi 2021; Laitinen et al. 2023; Bian et al. 2024), as well as observed variations in the HMF winding angle (e.g. Bieber 1988; Smith and Bieber 1991), which could lead to deviations in the expected nominal Parker field geometry, and hence to potentially erroneous warnings. As such, SEP transport models require reliable, and above all realistic, modelling of the plasma environment that these particles encounter. The present study aims to contribute to this effort by providing a longer term analysis of the winding angle, and hence geometry, of the heliospheric magnetic field than presented in prior studies, using almost 60 years of spacecraft observations at 1 AU, and by investigating the influence of turbulence thereon.

The Parker (1958) HMF model has long been known to provide a reasonably accurate description of the large-scale HMF (see, e.g., Burlaga et al. 1982; Bruno and Bavassano 1997), albeit in the solar ecliptic plane. At higher latitudes alternative models for the HMF have been proposed (e.g. Fisk 1996; Schwadron 2002; Hitge and Burger 2010; Steyn and Burger 2020), but these are not considered here. As such, the Parker HMF normalised to the value of its radial component $B_{0,r}$ at Earth r_e is given in heliocentric spherical polar coordinates by

$$\mathbf{B}_0 = \left|B_{0,r}(r_e)\right| \left(\frac{r_e}{r}\right)^2 [\hat{e}_r - \tan\psi \hat{e}_\phi] \tag{1}$$

where ψ denotes the winding angle of the spiral HMF lines,

$$\tan\psi_P = -\frac{B_\phi}{B_r} \tag{2}$$

$$= \frac{\Omega_S}{v_{sw}}(r - R_A)\sin\theta, \tag{3}$$

which nominally is expected for a purely Parker field to assume a value of $\approx 45^\circ$ for a solar wind speed of $v_{sw} = 400$ km/s, with Ω_S the sidereal rotation frequency of the Sun's equator. Note that this definition differs from the definition of Ω used in Equation 4. The quantity R_A denotes the Alfvén point height, where it is assumed that the frozen-in flow condition is initially met. Typically, the estimates within which the value of this quantity vary, with Lotova, Blums, and Vladimirskii (1985) finding a range of $10-30\ r_\odot$, while Goelzer, Schwadron, and Smith (2014) reported values ranging from $15-30\ r_\odot$, with a potential solar cycle dependence. Kasper and Klein (2019) found a typical value of $R_A \approx 25\ r_\odot$ and a strong solar cycle dependence of this quantity. Recently, Parker Solar Probe observations have provided

[1] The minimum energy transit between Earth and Mars; see, e.g., Curtis (2014).

revised estimates of this quantity, where several studies report values of $\approx 16\, r_\odot$ (e.g. Kasper et al. 2021; Bandyopadhyay et al. 2022), although this is expected to vary (Chhiber et al. 2022). In what follows, the present study assumes a compromise value of $R_A = 20\, r_\odot$, given the temporal range of data analysed, and an uncertainty window ranging between $10-40\, r_\odot$ is generated based on the typical variability of helioradii where sub-Alfvénic flows transition to super-Alfvénic flows in the solar atmosphere (Chhiber et al. 2024).

Relatively few studies have in the past investigated the winding of the 2D Parker HMF lines at Earth. Bieber (1988) analysed 20 years of spacecraft observations, reporting that the HMF was on average overwound relative to the nominal $\psi_P \approx 45^\circ$ expected of the Parker field. Furthermore, this author reported a North-South asymmetry in the HMF winding angle, such that the HMF was more tightly wound North of the heliospheric current sheet. It was not explicitly reported whether this asymmetry persisted over multiple solar cycles and one cannot visually discern a solar cycle dependence from the reported figures, but it seems that the asymmetry does indeed persist over the two solar cycles for which data were available and is present during solar minimum and solar maximum, albeit to varying degrees, e.g. the asymmetry nearly disappeared at the 1965 and 1975 solar minima but was present at the 1970 and 1980 solar maxima. The asymmetry was confirmed by Smith and Bieber (1993), who extended the analysis by taking into account observations at radial distances greater than 1 AU from the Pioneer 10 and Voyager spacecraft. Smith and Bieber (1991) specifically considered the temporal dependence in the HMF winding angle, reporting this on average to be overwound from their analysis of 22 years of spacecraft observations, with the HMF being considerably more wound during solar maximum conditions than during solar minima. These authors argued that the overwinding of the HMF was due to nonzero azimuthal field components that arose from solar differential rotation which might be convected into the solar corona, thereby providing a possible source of azimuthal magnetic fields at the source point of the solar wind not taken into account in the Parker model, proposing a modification to the standard Parker HMF model to take this into account. Smith and Bieber (1991) also found that the solar cycle variations in the winding angle were mostly due to solar cycle variations in the solar wind speed. Lastly, Isaacs, Tessein, and Matthaeus (2015) also calculated the winding angle from observations, but with a focus on the influence of data averaging on the final result. The aforementioned studies all employed similar methods to compute the winding angle from observations, viz. directly from Equation 3, using the observed solar wind speed as a direct input. The present study aims to extend these analyses, taking into account the almost 60 years of spacecraft data now available, and to directly compute the winding angle from the observed HMF components using Equation 2. The HMF as observed by spacecraft is known to vary in all three dimensions, as opposed to the Parker HMF model, which has no meridional component. The meridional component of the observed HMF has long been associated with turbulence, and it is known that such turbulent fluctuations result in the meandering of the HMF lines (see, e.g., Matthaeus et al. 1995; Laitinen et al. 2023; Bian et al. 2024). The present study also aims to investigate this phenomenon by analysing spacecraft observations using the definition of the winding angle of a 3D HMF model proposed by Burger et al. (2008). As the additional data available will allow for a full investigation of any temporal periodicities in both 2D and 3D winding angles, these will also be investigated. The influence of HMF turbulence on the 3D winding angle is also investigated, using a simple model for turbulence transverse to the nominal Parker HMF. The question naturally arises as to whether such changes in HMF geometry would influence the focusing of charged particles such as solar energetic particles. Due to the invariance of the magnetic moment, an SEP moving away from the Sun, and hence experiencing a decreasing HMF magnitude, will experience a decrease in its speed perpendicular

to this field, and a corresponding increase in speed parallel to the HMF. In this process, its transport becomes more ballistic along the HMF (e.g. Earl 1976, 1981), which leads to the observed anisotropies of SEPs (Roelof 1969; Bieber, Evenson, and Pomerantz 1986; van den Berg, Strauss, and Effenberger 2020). The influence of turbulence on the focusing length of SEPs will be therefore also considered.

The subject of the following section is a discussion of the data analysis techniques employed here, after which the results of these analyses will be presented in Section 3. The influence of HMF turbulence on the 3D winding angle and magnetic focusing length is investigated in Section 4. The article ends with a section devoted to a discussion of the results presented here.

2. Data Analysis

For this analysis the hourly-averaged Low Resolution OMNI (LRO) data set (King and Papitashvili 2005) available on the NASA OMNIWeb website[2] is used, spanning approximately 60 years of data from 28 November 1963 up to 31 December 2023. The magnetic field parameters used in this study are the magnetic field components B_x, B_y, and B_z in units of nano-Tesla (nT) in the geocentric solar ecliptic (GSE) coordinate system, and the plasma flow speed v in units of km s^{-1}. The use of hourly resolution data is motivated by the need for comparison with the results reported by previous studies, such as that of Smith and Bieber (1991), who also employ hourly data in their analyses. Furthermore, it was demonstrated by Isaacs, Tessein, and Matthaeus (2015) that winding angles computed from data intervals averaged over longer intervals are relatively insensitive to the duration of the data averaging interval.

Bieber (1988) developed a method to designate a sector label to measurements of the HMF, and this method was employed in the study conducted by Smith and Bieber (1991, 1993) to which the analysis in this article is compared. The equation

$$\tan\psi_P = \frac{\Omega}{v}\sin\theta\left(1-\frac{R_A}{r}\right) \tag{4}$$

determines the expected orientation of the HMF based on the magnitude of the solar wind speed (plasma flow speed) and is used to determine the sector designation of an HMF vector. In Equation 4, ψ_P is the winding angle defined per the Parker theory, $\Omega = 2\pi r_\odot/T$ is the linear speed of the Sun's equator with T defined as the sidereal rotation period of the Sun's equator, θ is the colatitude of a magnetic footpoint on the source surface, R_A is the Alfvén point height as defined in Section 1 and r is the radial position of a point in the heliosphere. Note that this definition of Ω differs from the definition used in Equation 3. As Figure 1 of Bieber (1988) illustrates, the method assigns to each HMF vector either a toward or an away sector label, where the toward and away sectors are the half-planes in which an HMF vector resides with respect to a plane that is normal to the spiral direction predicted by the Parker model of the HMF.

The analysis performed in this study primarily computes the winding angles not from the solar wind speed, but rather from the magnetic field components. The two-dimensional winding angle is defined as

$$\tan\psi = -\frac{B_\phi}{B_r} \tag{5}$$

[2] https://omniweb.gsfc.nasa.gov/.

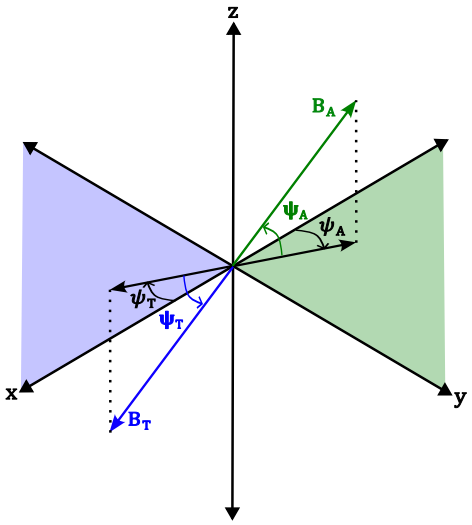

Figure 1 The vector geometry of arbitrary magnetic field vectors in the GSE coordinate system at 1 AU where the blue and green quadrants in the xy-plane are the towards and away sectors respectively as described in this section. The winding angles of the Parker field vectors, i.e. the projections of the magnetic field vectors onto the xy-plane, are measured relative to the positive and negative x-axis for the towards and away winding angles respectively. The 3D winding angles are defined as the angles between the magnetic field vectors and their projections in the xy-plane (see Figure 6 of Burger et al. 2008).

while Burger et al. (2008) provides a three-dimensional definition of the winding angle,

$$\tan\Psi = -\frac{B_\phi}{\sqrt{B_r^2 + B_\theta^2}} \tag{6}$$

where B_r, B_ϕ and B_θ are the radial, azimuthal, and meridional magnetic field components and ψ (and Ψ) is the winding angle calculated from the magnetic field components. Both definitions are in spherical coordinates and with the substitution $B_r = -B_x$, $B_\phi = -B_y$ and $B_\theta = B_z$ the two-dimensional (2D) definition becomes

$$\tan\psi = \frac{B_y}{B_x} \tag{7}$$

and the three-dimensional (3D) definition becomes

$$\tan\Psi = \frac{B_y}{\sqrt{B_x^2 + B_z^2}} \tag{8}$$

such that the winding angle definitions are recast into GSE coordinates as shown in Figure 1. The winding angle measurements are designated with a sector label based on the sign of the magnetic field components they were calculated from. In the two-dimensional magnetic field a measurement is denoted as towards (T) if B_x is positive and B_y is negative, while the opposite signs denote a measurement in the away (A) sector. For the three-dimensional magnetic field the B_z component can have any sign in addition to the previously mentioned sign convention for the two-dimensional magnetic field. Magnetic field measurements that fall into neither sector designation have been labeled as miscellaneous and excluded from the analysis.

The magnetic field measurements, corresponding winding angles, and solar wind speed data in each year are binned into 27-day bins. If the number of magnetic field measurements in a bin is less than 15% of the total measurements in the bin (including placeholder values), both the binned magnetic field data and corresponding solar wind speed data are

discarded. This allows for the most direct comparison between the winding angles that the Parker theory predicts with Equation 4, the winding angles calculated from the magnetic field components with Equation 7 and Equation 8, and with the results of Smith and Bieber (1991). To compute uncertainties on the winding angle values, we calculate the sample standard deviation on the winding angle values in each 27-day bin for each sector separately,

$$\sigma^2 = \frac{1}{n-1}\sum_{i=0}^{n}(\psi_i - \langle\psi\rangle)^2 \tag{9}$$

where ψ now represents either the 2D or 3D winding angle and n is the number of winding angle values per sector in each bin.

In each 27-day bin the toward and away winding angles are averaged separately, and the average of the two sectors is calculated as the average winding angle for the bin, as described by

$$\langle\psi \pm \sigma\rangle_{\text{per bin}} = \frac{1}{2}\left[(\langle\psi_A\rangle + \langle\psi_T\rangle) \pm \sqrt{\sigma^2_{SEM,A} + \sigma^2_{SEM,T}}\right] \tag{10}$$

where $\langle\psi_T\rangle$ and $\langle\psi_A\rangle$ are the average toward and away winding angles per bin, respectively, and

$$\sigma_{SEM,A} = \frac{\sigma_A}{\sqrt{n_A}},\ \sigma_{SEM,T} = \frac{\sigma_T}{\sqrt{n_T}} \tag{11}$$

are the standard errors on the mean winding angle for each sector. The solar wind speed data is averaged similarly according to

$$\langle v\rangle = \frac{\langle v_T\rangle + \langle v_A\rangle}{2} \tag{12}$$

with $\langle v_T\rangle$ and $\langle v_A\rangle$ the respective toward and away averages of the solar wind speed per bin. The averaged values of the 27-day bins in each year are then averaged to find the average winding angle per year with the errors on the winding angles described in Equation 10 propagated linearly and is given by the following equation

$$\langle\psi \pm \sigma\rangle_{\text{per year}} = \frac{1}{n}\left(\sum_{i=1}^{n}\psi_i \pm \sqrt{\sum_{i=1}^{n}\sigma_i^2}\right) \tag{13}$$

which is also used to calculate the average winding angle over the entire data range in this analysis. The subscript in Equation 13 is dropped in the rest of the text with the final average over the dataset instead reported using the notation $\langle\psi\rangle$ in the text and figures that follow.

Equation 4 is used to calculate the theoretical predictions for the winding angles with the average solar wind speed from Equation 12. Since the orbit of Earth is in the ecliptic plane of the Sun, the sinusoidal term in Equation 4 is taken to be unity, while the values of the remaining parameters are the same values used by Smith and Bieber (1991): the sidereal rotation period is $T = 25.4$ days, $r = 1$ AU is the Sun-Earth distance, and the Alfvén point height is $R_A = 20\ r_\odot$ as discussed in Section 1. The ecliptic plane in which Earth orbits is tilted with respect to the solar equatorial plane in which the winding angle of the Parker HMF is defined. This leads to a mixing between some of the magnetic field components, particularly at the equinoxes of Earth's orbit. However, since we only consider data that is

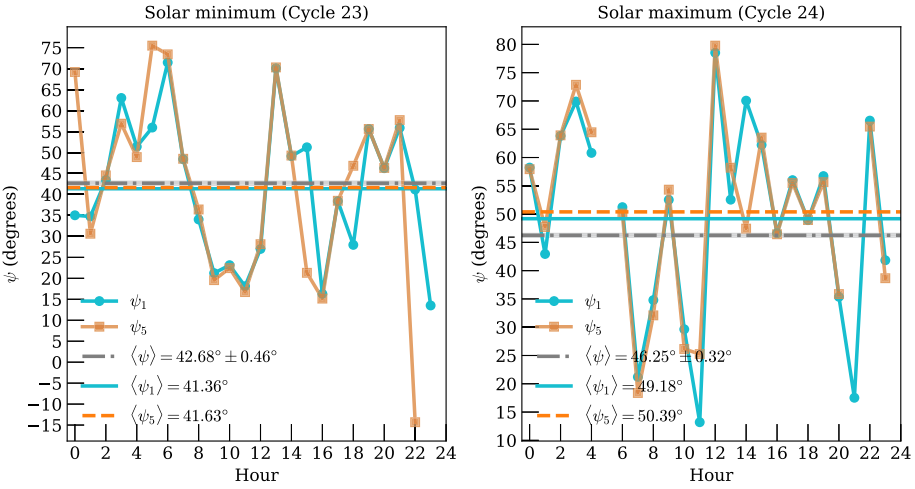

Figure 2 Winding angles calculated for a 24-hour interval of one-minute cadence (ψ_1, blue dots) (King and Papitashvili 2020a) and five-minute cadence (ψ_5, orange squares) (King and Papitashvili 2020b) OMNIWeb data at the solar minimum of Cycle 23 (1996-08-01, left panel) and at the solar maximum of Cycle 24 (2014-04-01, right panel). The grey dash-dotted line and uncertainty band in each panel is the average winding angle of the data from a particular year data as shown in Figure 3.

averaged over 27-day intervals and then subsequently averaged annually over those 27-day averaged intervals, this mixing effect should be averaged out enough over the course of one orbit that it would not have a significant effect on the winding angle results. Similarly, we make use of the average distance between Earth and the Sun when taking $r = 1$ AU, since this same averaging process would sufficiently average out variations in the winding angles calculated with Equation 4 due to relatively small variations in Earth's orbital distance.

We report on the over- or underwoundness of the HMF calculated from the spacecraft data relative to the Parker HMF in two ways: firstly we take the difference between the averages of the winding angles calculated from spacecraft data and the Parker winding angles over the entire dataset, that is,

$$\langle\psi\rangle - \langle\psi_P\rangle = \frac{1}{n}\left[\sum_{i=1}^{n}(\psi_i - \psi_{P,i}) \pm \sqrt{\sum_{i=1}^{n}\sigma_i^2}\right], \tag{14}$$

and secondly by taking the mean of the differences between the winding angles calculated from the spacecraft data and the Parker winding angles,

$$\langle|\psi_P - \psi|\rangle = \frac{1}{n}\left[\sum_{i=1}^{n}|\psi_{P,i} - \psi_i| \pm \sqrt{\sum_{i=1}^{n}\sigma_i^2}\right] \tag{15}$$

which is the method favoured to report the results in Figure 9.

It is not clear from Isaacs, Tessein, and Matthaeus (2015) what the influence of shorter data cadences on the calculated winding angles would be. Figure 2 shows 2D winding angles calculated over two 24-hour intervals, using one- and five-minute cadence OMNIWeb data for the solar minimum of Solar Cycle 23 (left panel) and the solar maximum of Solar

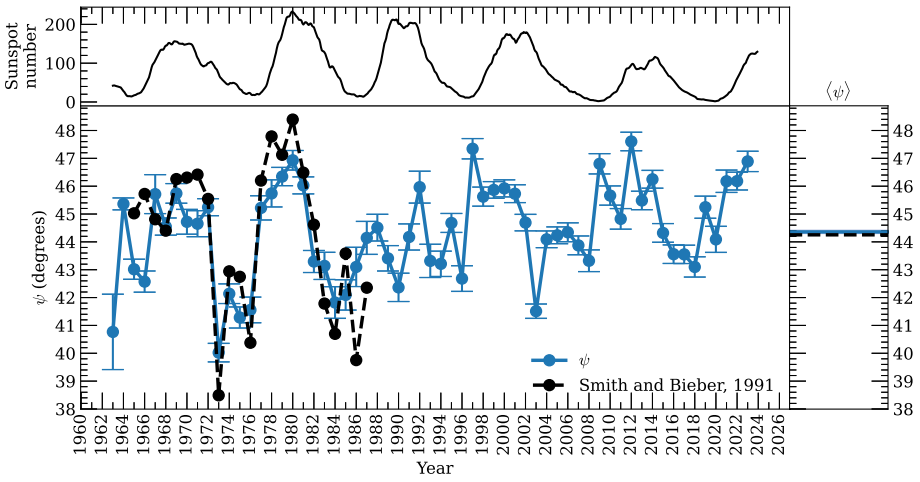

Figure 3 Yearly averaged 2D winding angles with their errors are calculated using Equation 13. The digitized results of Smith and Bieber (1991) for 1965 until 1987 are given by the dashed line as a means for comparison. The average winding angle of the two data sets is given in the right-hand side plot by the horizontal lines. The top panel shows the 13-month smoothed monthly total sunspot number (SILSO World Data Center 1963 – 2023) as a solar cycle index to which the winding angle results can be compared. Figures 4, 6, and 7 also use this solar cycle index.

Cycle 24 (right panel). Differences between the average winding angles for each case remain relatively small. The yearly averaged winding angle for each interval (see Figure 3 and its accompanying discussion) is also indicated on each panel of Figure 2. For the solar minimum interval, the yearly average is similar to the five- and one-minute cadence averages, while for solar maximum it is somewhat smaller.

A correlation between the winding angles calculated from the magnetic field data, as well as the predicted winding angles calculated from the solar wind speed, and the solar cycle was sought. The Lomb-Scargle periodogram (Lomb 1976; VanderPlas 2018) was employed with the PAST (PAleontological STatistics) statistical software (Hammer and Harper 2001) to obtain possible periodicities in the yearly averaged data corresponding to the 11- and 22-year solar cycles. This statistical method was chosen for its ability to extract periodicities from unevenly sampled data, which was necessary since the hourly sampled magnetic field data contained missing values, and the restriction on the number of measurements placed on the bins introduced further discontinuities in the yearly averaged winding angle data. Signals that were close to 11- or 22-year periodicities were only considered to be significant if the signal peak surpassed a p-value of $p < 0.01$, i.e. the signal surpassed the 99% confidence level.

3. Results

The results calculated from Equation 13 for the Parker HMF are presented in Figure 3 for the 60 year period from 1963 – 2023 along with the digitized results of Smith and Bieber (1991) for the period of 1965 – 1987 corresponding to their analysis. The top panel of Figure 3 (and subsequent figures) shows the 13-month smoothed monthly total sunspot number[3]

[3]Source: WDC-SILSO, Royal Observatory of Belgium, Brussels.

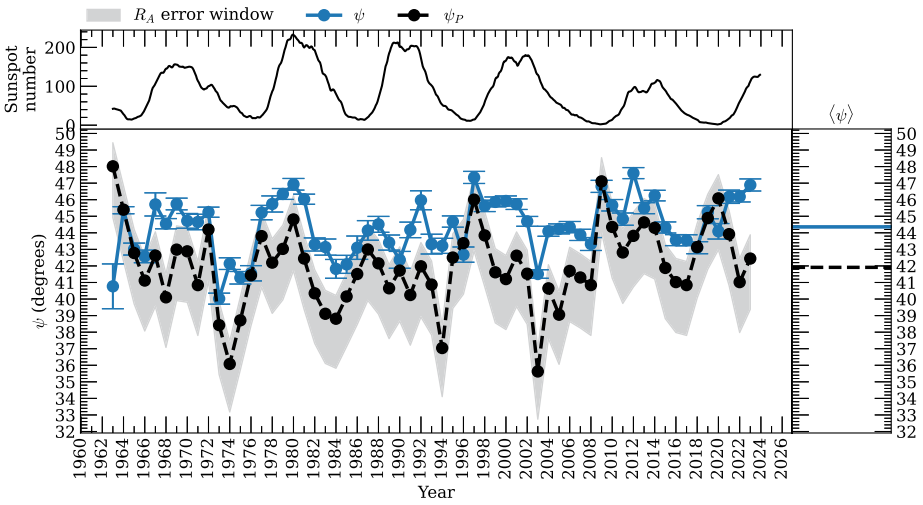

Figure 4 The 2D winding angle results from Figure 3 plotted against the winding angles predicted by the Parker model, given by Equation 4 for $R_A = 20\, r_\odot$, and an uncertainty window of the Parker winding angles for a range of Alfvén point heights from 10 $r_\odot$ (upper limit of window) to 40 $r_\odot$ (lower limit of window) with the solar wind speed given by Equation 12. The top panel shows the 13-month smoothed monthly total sunspot number as a solar cycle index.

as a proxy for solar activity levels. Smith and Bieber (1991) reported an average winding angle of 44.4° as is shown in the right-hand side of the figure. We extend the analysis to the full 60 year data set and report an average winding angle calculated from the magnetic field components of $44.36° \pm 0.06°$. Even though the average winding angles for both studies are in very good agreement, the results of the present study do not exactly match those of Smith and Bieber. Two possible reasons for this discrepancy are, firstly, that the present study employs a different method of averaging than the one that was employed in the aforementioned study, namely that we average over the winding angles calculated from the individual magnetic field measurements for the two sectors whereas Smith and Bieber (1991) calculated their winding angles from the vector sum of the unit vectors of the individual magnetic field measurements. The use of the slightly simpler averaging method in this study does not contribute greatly to the discrepancy in the results in Figure 3 since the two averaging methods give nearly identical results (see Figure 2 in Smith and Bieber 1991). Secondly, the method by which magnetic field measurements are given sector designations differ in this study and most likely contribute to the greater part of the discrepancy in the results. We employed a simpler sector designation method by simply assigning to a magnetic field vector a sector based on the signs of its components, whereas Smith and Bieber employed the method developed and described by Bieber (1988) where the sector designation was based on the orientation of a field measurement and its location within one of two half planes that are defined by the plane that is perpendicular to the Parker HMF.

Smith and Bieber (1991) further reported that their average winding angle mentioned previously is overwound from the nominal value of 41.6° predicted by the Parker model for a source surface distance of $R_A = 20\, r_\odot$. They did not report the exact number, but it was calculated from their results as 2.8°. Figure 4 shows the results of our study compared to the nominal winding angle values predicted by the Parker model for the same R_A and the averaged solar wind speeds given by Equation 12 and calculated from the LRO data set.

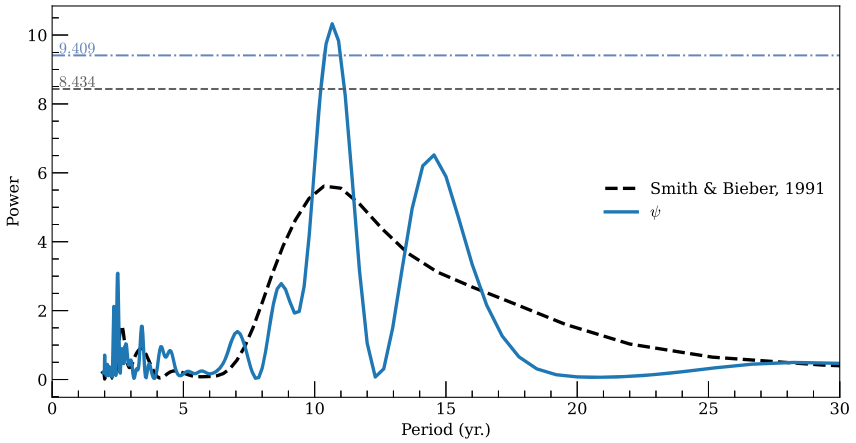

Figure 5 Lomb-Scargle periodogram of the 2D winding angle results and the results of Smith and Bieber (1991). The 99% confidence levels for each dataset are plotted as the horizontal lines.

As previously mentioned we calculate an average winding angle of $44.36° \pm 0.06°$ which is overwound from the nominal Parker winding angle of $41.91°$ by $2.45° \pm 0.06°$ per Equation 14, and overwound by $2.67° \pm 0.06°$ per Equation 15. This result is in good agreement with the overwound result of Smith and Bieber. Furthermore, strengthening our argument that this result is overwound, our results also lie for the most part above the uncertainty window on the winding angles predicted by the Parker model.

Figure 5 illustrates the periodogram for both the Smith and Bieber (1991) results as well as those obtained in the present study, with horizontal lines denoting 99% confidence levels for their corresponding datasets. Due to the limited data available at the time of their study, the confidence level for the Smith and Bieber (1991) study is lower than the confidence level for our study with a much greater sample size. Their results show a clear peak corresponding to an ≈ 11 year periodicity, but below 99% confidence. The results from this study show two clear peaks: at an ≈ 11 year periodicity, as well as at a possible ≈ 15 year periodicity. It should, however, be noted that only the ≈ 11 year peak is statistically significant.

Figure 6 and Figure 7 show the yearly averaged winding angles of the away and towards sectors respectively for the 3D HMF defined by Equation 8. The away average winding angle is $38.65° \pm 0.06°$, underwound from the nominal Parker value of $41.91°$ by $3.26° \pm 0.06°$, while the towards average winding angle is $-39.25° \pm 0.07°$, underwound by $2.66° \pm 0.07°$. Calculating the mean of the differences between the nominal Parker winding angles and the 3D winding angles with Equation 15, the away winding angle is underwound by $3.63° \pm 0.07°$ and the towards sector is underwound by $2.95° \pm 0.07°$. The 3D HMF is therefore on average underwound by $\approx 3°$. In both cases our results are also mostly underwound with respect to the uncertainty window on the Parker winding angles as well. Note that the averaged winding angle values for the towards sector in Figure 7 are negative because the sign of B_y is negative in that sector and the deviation of the average value from the nominal Parker winding angle is calculated with the absolute value of the T sector average.

An unexpected result is the lack of strong periodic signals in the data for the 3D winding angles, for both the towards and away sectors, as shown in the periodogram of Figure 8. There are no ≈ 11 year or ≈ 15 year periodicities that exceed the 99% confidence level plotted in that figure. A possible reason for this is explored in the next section.

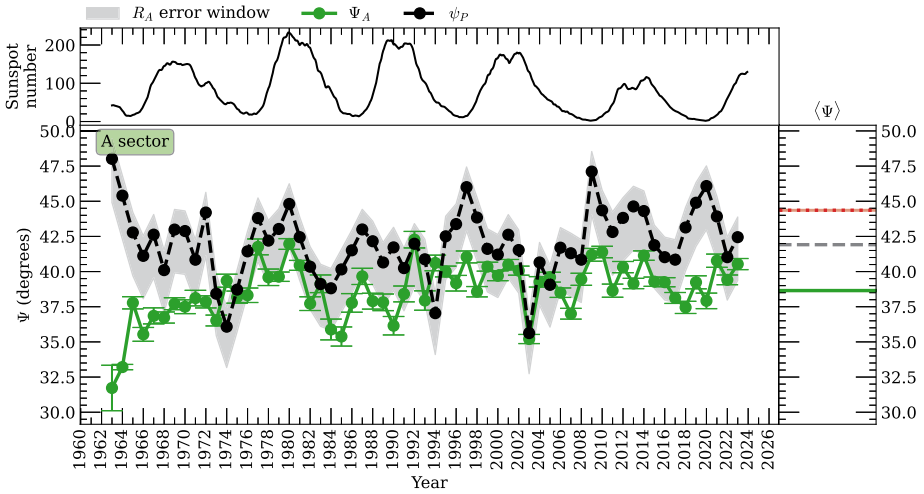

Figure 6 Yearly averaged 3D winding angles for the away sector calculated from Equation 8. The winding angles predicted by the Parker model as shown in Figure 4 are also plotted here, clearly showing the underwinding of the 3D field with respect to the nominal Parker field. The red dotted line in the right panel is $\langle\psi\rangle$ as reported in Figure 4.

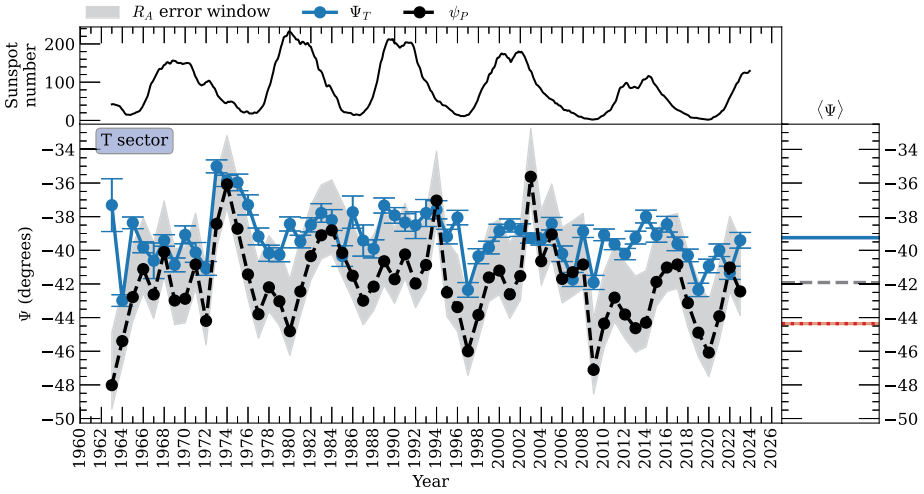

Figure 7 Yearly averaged 3D winding angles for the toward sector calculated from Equation 8 with the winding angles predicted by the Parker model plotted for comparison. The underwinding of the T sector is also evident compared to the nominal Parker field. Note that the sign of the winding angles predicted by the Parker model is inverted to provide a better comparison since the magnetic field vectors of the T sector point towards the Sun while the field vectors of the Parker model (after averaging the two sectors) primarily point away from the Sun.

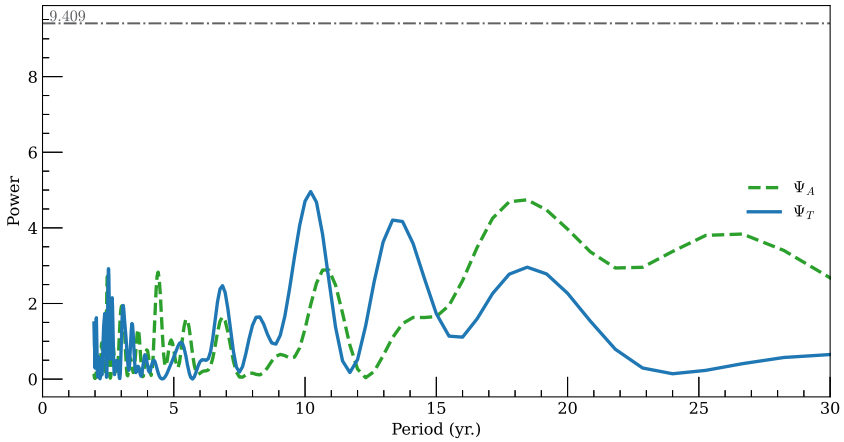

Figure 8 Lomb-Scargle periodogram of the 3D winding angle results for both the towards and away sectors. The horizontal line again denotes the 99% confidence level.

4. The Influence of Turbulence and the Consequences for Magnetic Focusing

Given the average underwound winding angle found when calculating this quantity as defined for a 3D HMF, the question arises as to whether HMF turbulence transverse to the Parker field could be playing a role in this phenomenon. This is due to two reasons. Firstly, in the Parker model, a non-zero meridional HMF component with a long-term zero average would most likely represent a contribution from turbulent magnetic fluctuations transverse to the background HMF (see, e.g., Burger, Nel, and Engelbrecht 2022). Secondly, Bian et al. (2024) demonstrated that the random walk of magnetic field lines (due to turbulence) would result in an underwound HMF. In order to investigate this, we define the full 3D field to be a Taylor-decomposed (Taylor 1935) sum of a uniform background component B_0, described by the Parker field, and two transverse fluctuating components b_1 and b_2, such that

$$\mathbf{B} = B_0\hat{e}_B + b_1\hat{e}_1 + b_2\hat{e}_2. \tag{16}$$

This approach requires an orthonormal basis in order to describe a turbulence geometry transverse to the Parker field itself. Such a basis can be defined as

$$\begin{aligned}\hat{e}_B &= \cos\psi_P\hat{e}_r - \sin\psi_P\hat{e}_\phi \\ \hat{e}_1 &= \hat{e}_\theta \\ \hat{e}_2 &= \hat{e}_B \times \hat{e}_\theta = \sin\psi_P\hat{e}_r + \cos\psi_P\hat{e}_\phi,\end{aligned} \tag{17}$$

where ψ_P again denotes the standard Parker winding angle given in Equation 5. The 3D magnetic field becomes

$$\mathbf{B} = (B_0\cos\psi_P + b_2\sin\psi_P)\hat{e}_r + b_1\hat{e}_\theta + (b_2\cos\psi_P - B_0\sin\psi_P)\hat{e}_\phi \tag{18}$$

with a winding angle of

$$\tan\psi' = \frac{B_0\sin\psi_P - b_2\cos\psi_P}{\left[(B_0\cos\psi_P + b_2\sin\psi_P)^2 + b_1^2\right]^{1/2}}. \tag{19}$$

Assuming axisymmetric fluctuations with relatively low strength relative to the background Parker HMF magnitude, as observed in the very inner heliosphere (see, e.g., Bruno and Carbone 2013; Adhikari et al. 2020; Chen et al. 2020), such that $\langle b_1^2 \rangle \approx \langle b_2^2 \rangle \approx \delta B_1^2$ with $B_0 b_1$ and $B_0 b_2$ being negligibly small, allows one to write

$$\begin{aligned} \tan\psi' &= \frac{B_0 \sin\psi_P}{\left[B_0^2 \cos^2\psi_P + \frac{1}{2}\delta B_1^2 (1+\sin^2\psi_P)\right]^{1/2}} \\ &\approx \tan\psi_P \left[1 + \frac{1}{2}\frac{\delta B_1^2}{B_0^2}\left(\frac{1+\sin^2\psi_P}{\cos^2\psi_P}\right)\right]^{-1/2}. \end{aligned} \tag{20}$$

Taking the inverse tangent on both sides of Equation 20 gives the winding angle due to turbulence for which the uncertainty on that winding angle can be determined as

$$\begin{aligned} \sigma_{\psi'} &= \sqrt{\left(\frac{\partial\psi'}{\partial(\delta B_1/B_0)}\right)^2 \sigma(\delta B_1/B_0)^2} \\ &= \left[\frac{\left[\frac{1}{2}\tan\psi_P \left(\frac{\delta B_1}{B_0}\right)\left(\frac{1+\sin^2\psi_P}{\cos^2\psi_P}\right)\right]^2 \sigma(\delta B_1/B_0)^2}{\left[1+\frac{1}{2}\frac{\delta B_1^2}{B_0^2}\left(\frac{1+\sin^2\psi_P}{\cos^2\psi_P}\right)\right]\left[1+\tan^2\psi_P+\frac{1}{2}\frac{\delta B_1^2}{B_0^2}\left(\frac{1+\sin^2\psi_P}{\cos^2\psi_P}\right)\right]^2}\right]^{\frac{1}{2}} \end{aligned} \tag{21}$$

The above expressions can then be evaluated using as inputs for the magnetic variance δB_1^2 from observations and the uncertainty on the magnetic variance relative to the background magnetic field magnitude $\sigma(\delta B_1/B_0)$. This was done for magnetic variances (and their uncertainties) reported by Burger, Nel, and Engelbrecht (2022) over the time interval of interest to this study, using the values for ψ_P calculated here in Equation 20. The differences between winding angles calculated from solar wind observations for the Parker model and the 3D winding angles for both the towards and away sectors calculated from the HMF components are shown in Figure 9 as function of time. Average differences between the Parker prediction and the towards and away sector 3D angles are $2.95^\circ \pm 0.07^\circ$ and $3.63^\circ \pm 0.07^\circ$, denoted by blue and orange lines, respectively. The average difference between the Parker prediction and Equation 20 denoted by the green line is $4.19^\circ \pm 0.04^\circ$, relatively close to the abovementioned deviations, and similar to the $\approx 5^\circ$ underwinding reported by Bian et al. (2024) due to the turbulent meandering of Parker field lines. If these differences are calculated for the Parker model with $R_A = 0\ r_\odot$, then the average difference between the Parker prediction and the towards sector 3D averages is $5.59^\circ \pm 0.07^\circ$ and $6.21^\circ \pm 0.07^\circ$ for the away sector averages with the average difference between the Parker prediction and Equation 20 being $4.72^\circ \pm 0.05^\circ$ (these are not shown on the graph). It can therefore be concluded that transverse turbulence can play a role in the underwinding of the 3D HMF reported on here.

Solar energetic particle focusing can be influenced by the abovementioned changes in HMF geometry. This effect is quantified through the focusing length $L = [\nabla \cdot \hat{e}_B]^{-1}$ (Roelof 1969), vanishing in the limit of large values of L. For a purely Parker field, this quantity is given by (see, e.g., Bieber, Evenson, and Pomerantz 1986)

$$L = \frac{r}{\cos\psi_P (1+\cos^2\psi_P)}. \tag{22}$$

The influence of turbulence on L can be estimated by calculating the divergence of a unit vector $\hat{e}_{BT}$ along the total turbulent field described by Equation 16, which becomes after

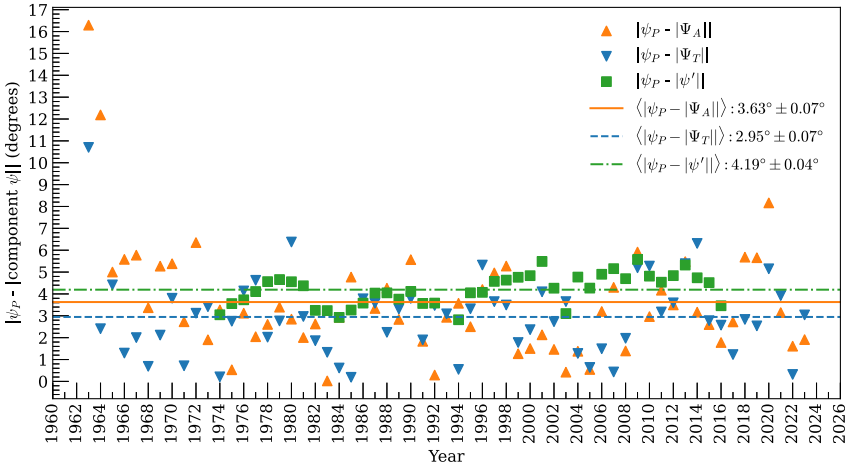

Figure 9 Differences between the Parker prediction for the winding angle and the 3D away and towards sector winding angles, and ψ' given by Equation 20, as functions of time. The average differences are indicated by the horizontal lines.

minor rearrangement

$$\hat{e}_{BT} = \frac{(\cos\psi_P + (b_2/B_0)\sin\psi_P)\hat{e}_r + (b_1/B_0)\hat{e}_\theta + ((b_2/B_0)\cos\psi_P - \sin\psi_P)\hat{e}_\phi}{\sqrt{1 + b_1^2/B_0^2 + b_2^2/B_0^2}}. \quad (23)$$

If a suitable temporal average of this quantity is taken, and axisymmetric transverse turbulent fluctuations are assumed, then $\langle b_1\rangle = \langle b_2\rangle = 0$, and $\langle b_1^2\rangle \approx \langle b_2^2\rangle \approx \delta B_1^2$, so that

$$\langle\hat{e}_{BT}\rangle \approx \frac{\cos\psi_P\hat{e}_r - \sin\psi_P\hat{e}_\phi}{\sqrt{1 + 2\delta B_1^2/B_0^2}} = f\hat{e}_B, \quad (24)$$

where $\hat{e}_B$ is defined as in Equation 17, and f is a turbulent modification factor. The turbulence-modified focusing length can then be calculated from

$$L' = [\nabla\cdot\langle\hat{e}_{BT}\rangle]^{-1} = \left[f\frac{\cos\psi_P(1+\cos^2\psi_P)}{r} + \nabla f\cdot\hat{e}_B\right]^{-1}, \quad (25)$$

which reduces to the standard Parker result of Equation 22 for the no turbulence case. As a first approach to evaluating Equation 25 in the ecliptic plane, we employ a simple radial scaling for the magnetic variance employed in prior studies (see, e.g., Burger et al. 2008; Engelbrecht and Wolmarans 2020), so that $2\delta B_1^2 = 12.5r^{-2.4}$, in units of nT^2, (following the observations reported by Zank, Matthaeus, and Smith 1996; Smith et al. 2001, 2006; Pine et al. 2020). The nominal Parker focusing length, as well as the turbulence-modified focusing length, are shown as functions of radial distance in the left panel of Figure 10, with the ratio of these quantities shown in the right panel. The turbulence-modified focusing length is only marginally larger, implying only a very slight reduction of magnetic focusing effects for SEPs.

It should be noted that increases in turbulence levels at higher latitudes as reported by, e.g., Forsyth et al. (1996) and Erdős and Balogh (2005), would enhance this effect somewhat.

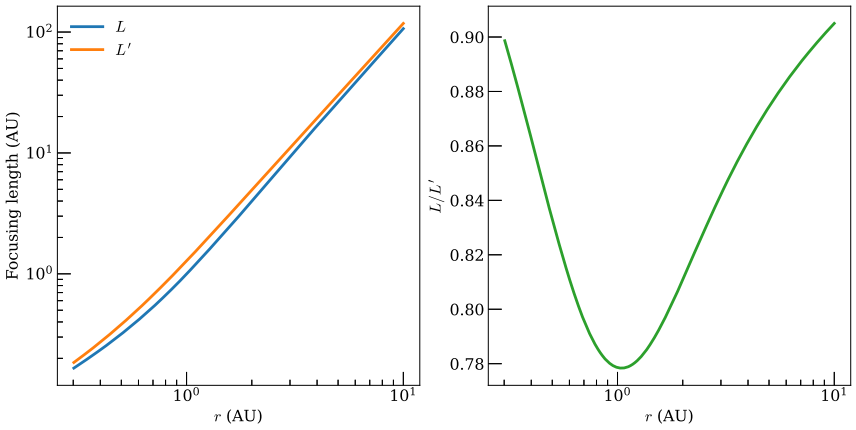

Figure 10 (left) The focusing length L of a purely Parker field and the turbulence-modified focusing length L' as a function of radial distance from 0.3 AU to 10 AU. (right) The ratio L/L' as a function of radial distance.

5. Discussion and Conclusions

The present study investigates the behaviour of the HMF winding angle over the past 60 years from spacecraft observations at 1 AU. The 2D winding angle here calculated agrees with the observations reported by Smith and Bieber (1991), being on average overwound as reported in that study, and displaying a clear solar cycle dependence, with overwound conditions corresponding to periods of high solar activity, and moderately underwound conditions corresponding to solar minimum periods. A Lomb-Scargle periodogram of the Smith and Bieber (1991) observations, spanning a period from 1965 – 1987, does reveal an ≈ 11 year periodicity, but well below the 99% confidence level. A periodogram of the results of our extended analysis also reveals this periodicity, but with a peak well above the 99% confidence level. Intriguingly, our results also indicate a potential ≈ 15 year periodicity in the 2D winding angle, but well below the 99% confidence level, which may simply be due to the fact that there is yet insufficient data to adequately sample this periodicity. Nevertheless, such longer term periodicities in the winding angle, and thus in the geometry of the HMF, may be of interest in studies of the longer term modulation of galactic cosmic rays (see, e.g., Caballero-Lopez et al. 2004; Cliver and Herbst 2018; Moloto and Engelbrecht 2020; Engelbrecht and Wolmarans 2020). Additionally, from a comparison of solar minimum results during the recent unusual solar minima (see, e.g., Li, Feng, and Wei 2021, and references therein) with those of other space-age solar minima, no discernible trend can be seen.

The 3D winding angle computed in this study, however, remains consistently underwound, albeit to a varying degree, over the whole data interval considered here. This result is consistent with what is expected from theory for field lines meandering due to turbulence (Bian et al. 2024). Furthermore, no significant periodicities can be discerned for this quantity. As the Parker field has no θ-component, the observed HMF component normal to the ecliptic plane must represent an additional, turbulent component, with the implication that HMF turbulence can be behind the underwinding of the 3D field. This can be demonstrated using a simple model of a 3D HMF, consisting of a Parker spiral field with two transverse, turbulently fluctuating components to calculate an analogous 3D winding angle that is both a function of the nominal Parker winding angle, and the turbulence magnetic variance

(Equation 20). In the presence of turbulence, such a model also yields a lower-than-nominal winding angle, and, when compared with observations, using as inputs observed magnetic variances at 1 AU reported by Burger, Nel, and Engelbrecht (2022), yields a deviation from the nominal winding angle not dissimilar to observations. Furthermore, Equation 20 can also explain the apparent lack of a solar cycle dependence in the observed 3D winding angle: it is a function of the ratio of the magnetic variance to the square of the HMF magnitude, a quantity that displays little to no solar cycle dependence due to the similar solar cycle dependencies of its components (Zhao et al. 2018; Burger, Nel, and Engelbrecht 2022).

Both the over and underwinding of the HMF at 1 AU can influence the efficacy of the Hohmann-Parker effect as a potential early warning for Mars missions as proposed by Posner et al. (2013): magnetic connectivity between the Earth and Mars may not be guaranteed. A possible amelioration of this would be careful modelling of SEP transport, taking into account the influence of turbulence on HMF lines. Such transport modelling would benefit greatly from the enhanced analysis of multiple spacecraft turbulence observations in the inner heliosphere, such as would be made possible by the proposed HelioSwarm mission (Klein et al. 2023). The present study proposes a relatively simple, yet effective, way of calculating the influence of turbulence on the winding of the HMF (Equation 20), by taking into account the observed magnetic variance, a quantity that is relatively simple to calculate from spacecraft observations (see, e.g., Forsyth et al. 1996). Changes in HMF geometry may also influence the focusing of SEPs. A relatively simple model for the influence of transverse turbulence on the focusing length is also presented here, and although it is demonstrated that this effect would not be large, it remains to be seen from direct SEP transport studies whether this would indeed be the case, given the greater relative significance of, e.g., diffusion effects on their transport (see, e.g., Strauss, Dresing, and Engelbrecht 2017; van den Berg et al. 2021). This will be the subject of future work.

Acknowledgments The authors acknowledge the use of NASA/GSFC Space Physics Data Facility's OMNIWeb service, and OMNI data. The OMNI data were obtained from the GSFC/SPDF OMNIWeb interface at https://omniweb.gsfc.nasa.gov. The authors further acknowledge the use of the Python libraries pandas (The pandas development team 2020), NumPy (Harris et al. 2020) and Matplotlib (Hunter 2007). The authors would like to thank an anonymous reviewer for valuable comments that greatly improved this study.

Author Contributions The study was conceived by N.E.E. and data acquisition and analysis were done by F.H. Figures 1 – 10 were prepared by F.H., with N.E.E. aiding in the preparation of Figure 9 and Figure 10. Both authors wrote the main manuscript text, and reviewed and approved the manuscript.

Funding Information Open access funding provided by North-West University. This work is based on the research supported partly by the National Research Foundation of South Africa (NRF grant number 137793). Opinions expressed and conclusions arrived at are those of the authors and are not necessarily to be attributed to the NRF. This research was supported by the International Space Science Institute (ISSI) in Bern, through ISSI International Team project #24-608 (Energetic Particle Transport in Space Plasma Turbulence).

Data Availability Data sets generated during the current study are available from the corresponding author on reasonable request.

Declarations

Competing Interests The authors declare no competing interests.

Open Access This article is licensed under a Creative Commons Attribution 4.0 International License, which permits use, sharing, adaptation, distribution and reproduction in any medium or format, as long as you give appropriate credit to the original author(s) and the source, provide a link to the Creative Commons licence, and indicate if changes were made. The images or other third party material in this article are included in the

article's Creative Commons licence, unless indicated otherwise in a credit line to the material. If material is not included in the article's Creative Commons licence and your intended use is not permitted by statutory regulation or exceeds the permitted use, you will need to obtain permission directly from the copyright holder. To view a copy of this licence, visit http://creativecommons.org/licenses/by/4.0/.

References

Adhikari, L., Zank, G.P., Zhao, L.-L., Kasper, J.C., Korreck, K.E., Stevens, M., Case, A.W., Whittlesey, P., Larson, D., Livi, R., Klein, K.G.: 2020, Turbulence transport modeling and first orbit Parker Solar Probe (PSP) observations. *Astrophys. J. Suppl. Ser.* **246**, 38. DOI. ADS.

Bandyopadhyay, R., Matthaeus, W.H., McComas, D.J., Chhiber, R., Usmanov, A.V., Huang, J., Livi, R., Larson, D.E., Kasper, J.C., Case, A.W., Stevens, M., Whittlesey, P., Romeo, O.M., Bale, S.D., Bonnell, J.W., Dudok de Wit, T., Goetz, K., Harvey, P.R., MacDowall, R.J., Malaspina, D.M., Pulupa, M.: 2022, Sub-Alfvénic solar wind observed by the Parker Solar Probe: characterization of turbulence, anisotropy, intermittency, and switchback. *Astrophys. J. Lett.* **926**, L1. DOI. ADS.

Barthel, J., Sarigul-Klijn, N.: 2019, A review of radiation shielding needs and concepts for space voyages beyond Earth's magnetic influence. *Prog. Aerosp. Sci.* **110**, 100553. DOI. ADS.

Bian, N.H., Strauss, R.D., Li, G., Engelbrecht, N.E.: 2024, Heliospheric diffusion of stochastic Parker spirals in radially evolving solar wind turbulence. *Astrophys. J.* **962**, 186. DOI. ADS.

Bieber, J.W.: 1988, North-South asymmetry of the interplanetary magnetic field spiral. *J. Geophys. Res.* **93**, 5903. DOI.

Bieber, J.W., Evenson, P.A., Pomerantz, M.A.: 1986, Focusing anisotropy of solar cosmic rays. *J. Geophys. Res.* **91**, 8713. DOI. ADS.

Bruno, R., Bavassano, B.: 1997, On the winding of the IMF spiral for slow and fast wind within the inner heliosphere. *Geophys. Res. Lett.* **24**, 2267. DOI. _eprint. https://onlinelibrary.wiley.com/doi/abs/10.1029/97GL02183.

Bruno, R., Carbone, V.: 2013, The solar wind as a turbulence laboratory. *Living Rev. Sol. Phys.* **10**, 1.

Burger, R.A., Nel, A.E., Engelbrecht, N.E.: 2022, Spectral properties of the N component of the heliospheric magnetic field from IMP and ACE observations for 1973 – 2020. *Astrophys. J.* **926**, 128. DOI. ADS.

Burger, R., Krüger, T., Hitge, M., Engelbrecht, N.: 2008, A Fisk-Parker hybrid heliospheric magnetic field with a solar-cycle dependence. *Astrophys. J.* **674**, 511.

Burlaga, L., Lepping, R., Behannon, K., Klein, L., Neubauer, F.: 1982, Large-scale variations of the interplanetary magnetic field: Voyager 1 and 2 observations between 1 – 5 AU. *J. Geophys. Res. Space Phys.* **87**, 4345.

Caballero-Lopez, R.A., Moraal, H., McCracken, K.G., McDonald, F.B.: 2004, The heliospheric magnetic field from 850 to 2000 AD inferred from ^{10}Be records. *J. Geophys. Res. Space Phys.* **109**, A12102. DOI. ADS.

Chen, C.H.K., Bale, S.D., Bonnell, J.W., Borovikov, D., Bowen, T.A., Burgess, D., Case, A.W., Chandran, B.D.G., de Wit, T.D., Goetz, K., Harvey, P.R., Kasper, J.C., Klein, K.G., Korreck, K.E., Larson, D., Livi, R., MacDowall, R.J., Malaspina, D.M., Mallet, A., McManus, M.D., Moncuquet, M., Pulupa, M., Stevens, M.L., Whittlesey, P.: 2020, The evolution and role of solar wind turbulence in the inner heliosphere. *Astrophys. J. Suppl. Ser.* **246**, 53. DOI. ADS.

Chhiber, R., Matthaeus, W.H., Usmanov, A.V., Bandyopadhyay, R., Goldstein, M.L.: 2022, An extended and fragmented Alfvén zone in the young solar wind. *Mon. Not. R. Astron. Soc.* **513**, 159. DOI. ADS.

Chhiber, R., Pecora, F., Usmanov, A.V., Matthaeus, W.H., Goldstein, M.L., Roy, S., Wang, J., Thepthong, P., Ruffolo, D.: 2024, The Alfvén transition zone observed by the Parker Solar Probe in young solar wind – global properties and model comparisons. *Mon. Not. R. Astron. Soc. Lett.* **533**, L70. DOI. ADS.

Cliver, E.W., Herbst, K.: 2018, Evolution of the sunspot number and solar wind B time series. *Space Sci. Rev.* **214**, 56. DOI. ADS.

Curtis, H.D.: 2014, *Orbital Mechanics for Engineering Students*. Elsevier. DOI ISBN 978-0-08-097747-8.

Earl, J.A.: 1976, The effect of adiabatic focusing upon charged-particle propagation in random magnetic fields. *Astrophys. J.* **205**, 900. DOI. ADS.

Earl, J.A.: 1981, Analytical description of charged particle transport along arbitrary guiding field configurations. *Astrophys. J.* **251**, 739. DOI. ADS.

Engelbrecht, N.E., Wolmarans, C.P.: 2020, Towards a deeper understanding of historic cosmic ray modulation during solar cycle 20. *Adv. Space Res.* **66**, 2722. DOI. ADS.

Engelbrecht, N.E., Effenberger, F., Florinski, V., Potgieter, M., Ruffolo, D., Chhiber, R., Usmanov, A., Rankin, J., Els, P.: 2022, Theory of cosmic ray transport in the heliosphere. *Space Sci. Rev.* **218**, 33.

Engell, A.J., Falconer, D.A., Schuh, M., Loomis, J., Bissett, D.: 2017, SPRINTS: a framework for solar-driven event forecasting and research. *Space Weather* **15**, 1321. DOI. ADS.

Erdős, G., Balogh, A.: 2005, In situ observations of magnetic field fluctuations. *Adv. Space Res.* **35**, 625. DOI. ADS.

Fisk, L.: 1996, Motion of the footpoints of heliospheric magnetic field lines at the Sun: implications for recurrent energetic particle events at high heliographic latitudes. *J. Geophys. Res. Space Phys.* **101**, 15547.

Forsyth, R.J., Horbury, T.S., Balogh, A., Smith, E.J.: 1996, Hourly variances of fluctuations in the heliospheric magnetic field out of the ecliptic plane. *Geophys. Res. Lett.* **23**, 595. DOI. ADS.

Goelzer, M.L., Schwadron, N.A., Smith, C.W.: 2014, An analysis of Alfvén radius based on sunspot number from 1749 to today. *J. Geophys. Res. Space Phys.* **119**, 115.

Guo, J., Zeitlin, C., Wimmer-Schweingruber, R.F., Hassler, D.M., Ehresmann, B., Rafkin, S., Freiherr von Forstner, J.L., Khaksarighiri, S., Liu, W., Wang, Y.: 2021, Radiation environment for future human exploration on the surface of Mars: the current understanding based on MSL/RAD dose measurements. *Astron. Astrophys. Rev.* **29**, 8. DOI. ADS.

Hammer, Ø., Harper, D.A.: 2001, Past: paleontological statistics software package for educaton and data anlysis. *Palaeontol. Electronica* **4**, 1.

Harris, C.R., Millman, K.J., van der Walt, S.J., Gommers, R., Virtanen, P., Cournapeau, D., Wieser, E., Taylor, J., Berg, S., Smith, N.J., Kern, R., Picus, M., Hoyer, S., van Kerkwijk, M.H., Brett, M., Haldane, A., del Río, J.F., Wiebe, M., Peterson, P., Gérard-Marchant, P., Sheppard, K., Reddy, T., Weckesser, W., Abbasi, H., Gohlke, C., Oliphant, T.E.: 2020, Array programming with NumPy. *Nature* **585**, 357. DOI.

Hitge, M., Burger, R.A.: 2010, Cosmic ray modulation with a Fisk-type heliospheric magnetic field and a latitude-dependent solar wind speed. *Adv. Space Res.* **45**, 18. DOI. ADS.

Hunter, J.D.: 2007, Matplotlib: a 2D graphics environment. *Comput. Sci. Eng.* **9**, 90. DOI.

Isaacs, J.J., Tessein, J.A., Matthaeus, W.H.: 2015, Systematic averaging interval effects on solar wind statistics. *J. Geophys. Res. Space Phys.* **120**, 868. DOI. _eprint. https://onlinelibrary.wiley.com/doi/pdf/10.1002/2014JA020661.

Kasper, J.C., Klein, K.G.: 2019, Strong preferential ion heating is limited to within the solar Alfvén surface. *Astrophys. J. Lett.* **877**, L35. DOI.

Kasper, J.C., Klein, K.G., Lichko, E., et al.: 2021, *Phys. Rev. Lett.* **127**. DOI.

King, J., Papitashvili, N.: 2005, Solar wind spatial scales in and comparisons of hourly Wind and ACE plasma and magnetic field data. *J. Geophys. Res. Space Phys.* **110**.

King, J.H., Papitashvili, N.E.: 2020a, OMNI 1-min Data Set, NASA Space Physics Data Facility. DOI.

King, J.H., Papitashvili, N.E.: 2020b, OMNI 5-min Data Set, NASA Space Physics Data Facility. DOI.

Klein, K.G., Spence, H., Alexandrova, O., Argall, M., Arzamasskiy, L., Bookbinder, J., Broeren, T., Caprioli, D., Case, A., Chandran, B., Chen, L.-J., Dors, I., Eastwood, J., Forsyth, C., Galvin, A., Genot, V., Halekas, J., Hesse, M., Hine, B., Horbury, T., Jian, L., Kasper, J., Kretzschmar, M., Kunz, M., Lavraud, B., Le Contel, O., Mallet, A., Maruca, B., Matthaeus, W., Niehof, J., O'Brien, H., Owen, C., Retinò, A., Reynolds, C., Roberts, O., Schekochihin, A., Skoug, R., Smith, C., Smith, S., Steinberg, J., Stevens, M., Szabo, A., TenBarge, J., Torbert, R., Vasquez, B., Verscharen, D., Whittlesey, P., Wickizer, B., Zank, G., Zweibel, E.: 2023, HelioSwarm: a multipoint, multiscale mission to characterize turbulence. *Space Sci. Rev.* **219**, 74. DOI. ADS.

Laitinen, T., Dalla, S., Waterfall, C.O.G., Hutchinson, A.: 2023, An analytical model of turbulence in Parker spiral geometry and associated magnetic field line lengths. *Astrophys. J.* **943**, 108. DOI. ADS.

Li, H., Feng, X., Wei, F.: 2021, Is solar minimum 24/25 another unusual one? *Astrophys. J. Lett.* **917**, L26. DOI. ADS.

Lomb, N.R.: 1976, Least-squares frequency analysis of unequally spaced data. *Astrophys. Space Sci.* **39**, 447.

Lotova, N., Blums, D., Vladimirskii, K.: 1985, Interplanetary scintillation and the structure of the solar wind transonic region. *Astron. Astrophys.* **150**(2), 266. ISSN 0004-6361.

Matthaeus, W.H., Gray, P.C., Pontius, J.D.H., Bieber, J.W.: 1995, Spatial structure and field-line diffusion in transverse magnetic turbulence. *Phys. Rev. Lett.* **75**, 2136. DOI. ADS.

Moloto, K.D., Engelbrecht, N.E.: 2020, A fully time-dependent Ab initio cosmic-ray modulation model applied to historical cosmic-ray modulation. *Astrophys. J.* **894**, 121. DOI. ADS.

Parker, E.N.: 1958, Dynamics of the interplanetary gas and magnetic fields. *Astrophys. J.* **128**, 664. DOI.

Pine, Z.B., Smith, C.W., Hollick, S.J., Argall, M.R., Vasquez, B.J., Isenberg, P.A., Schwadron, N.A., Joyce, C.J., Sokół, J.M., Bzowski, M., Kubiak, M.A., McLaurin, M.L.: 2020, Solar wind turbulence from 1 to 45 au. IV. Turbulent transport and heating of the solar wind using Voyager observations. *Astrophys. J.* **900**, 94. DOI. ADS.

Posner, A., Strauss, R.D.: 2020, Warning time analysis from SEP simulations of a two-tier REleASE system applied to Mars exploration. *Space Weather* **18**, e02354. DOI. ADS.

Posner, A., Odstrĉil, D., MacNeice, P., Rastaetter, L., Zeitlin, C., Heber, B., Elliott, H., Frahm, R.A., Hayes, J.J.E., von Rosenvinge, T.T., Christian, E.R., Andrews, J.P., Beaujean, R., Böttcher, S., Brinza, D.E., Bullock, M.A., Burmeister, S., Cucinotta, F.A., Ehresmann, B., Epperly, M., Grinspoon, D., Guo, J., Hassler, D.M., Kim, M.-H., Köhler, J., Kortmann, O., Martin Garcia, C., Müller-Mellin, R., Neal, K., Rafkin, S.C.R., Reitz, G., Seimetz, L., Smith, K.D., Tyler, Y., Weigle, E., Wimmer-Schweingruber, R.F.: 2013, The Hohmann-Parker effect measured by the Mars Science Laboratory on the transfer from Earth to Mars: consequences and opportunities. *Planet. Space Sci.* **89**, 127. DOI. ADS.

Ragot, B.R.: 2011, Statistics of field-line dispersal: random-walk characterization and supradiffusive regime. *Astrophys. J.* **728**, 50. DOI. ADS.

Roelof, E.C.: 1969, Propagation of solar cosmic rays in the interplanetary magnetic field. In: Ögelman, H., Wayland, J.R. (eds.) *Lectures in High-Energy Astrophysics* **111**. ADS.

Ruffolo, D., Chuychai, P., Matthaeus, W.H.: 2006, Random walk of magnetic field lines in nonaxisymmetric turbulence. *Astrophys. J.* **644**, 971. DOI. ADS.

Schwadron, N.A.: 2002, An explanation for strongly underwound magnetic field in co-rotating rarefaction regions and its relationship to footpoint motion on the the sun. *Geophys. Res. Lett.* **29**, 1663. DOI. ADS.

Schwadron, N.A., Blake, J.B., Case, A.W., Joyce, C.J., Kasper, J., Mazur, J., Petro, N., Quinn, M., Porter, J.A., Smith, C.W., Smith, S., Spence, H.E., Townsend, L.W., Turner, R., Wilson, J.K., Zeitlin, C.: 2014, Does the worsening galactic cosmic radiation environment observed by CRaTER preclude future manned deep space exploration? *Space Weather* **12**, 622. DOI. ADS.

Shalchi, A.: 2021, Field line random walk in magnetic turbulence. *Phys. Plasmas* **28**, 120501. DOI. ADS.

SILSO World Data Center: 1963 – 2023, The International Sunspot Number. *International Sunspot Number Monthly Bulletin and online catalogue*. http://www.sidc.be/silso/.

Slaba, T.C.: 2021, Historical reconstruction of astronaut cancer risk: context for recent solar minima. *Space Weather* **19**, e02851. DOI. ADS.

Smith, C.W., Bieber, J.W.: 1991, Solar cycle variation of the interplanetary magnetic field spiral. *Astrophys. J.* **370**, 435. DOI. MAG ID: 2087812249.

Smith, C.W., Bieber, J.W.: 1993, Multiple spacecraft survey of the North-South asymmetry of the interplanetary magnetic field. *J. Geophys. Res.* **98**. DOI. MAG ID: 2017814817.

Smith, C.W., Matthaeus, W.H., Zank, G.P., Ness, N.F., Oughton, S., Richardson, J.D.: 2001, Heating of the low-latitude solar wind by dissipation of turbulent magnetic fluctuations. *J. Geophys. Res.* **106**, 8253.

Smith, C.W., Isenberg, P.A., Matthaeus, W.H., Richardson, J.D.: 2006, Turbulent heating of the solar wind by newborn interstellar pickup protons. *Astrophys. J.* **638**, 508.

Steyn, P., Burger, R.: 2020, A generalized Fisk-type HMF: implications of spatially dependent photospheric differential rotation. *Astrophys. J.* **902**, 33.

Strauss, R.D.T., Dresing, N., Engelbrecht, N.E.: 2017, Perpendicular diffusion of solar energetic particles: model results and implications for electrons. *Astrophys. J.* **837**, 43. DOI. ADS.

Taylor, G.I.: 1935, Statistical theory of turbulence. *Proc. R. Soc. Lond. Ser. A* **151**, 421. DOI. ADS.

The pandas development team: 2020, pandas-dev/pandas: Pandas. Zenodo. DOI.

van den Berg, J., Strauss, D.T., Effenberger, F.: 2020, A primer on focused solar energetic particle transport. *Space Sci. Rev.* **216**, 146. DOI. ADS.

van den Berg, J.P., Engelbrecht, N.E., Wijsen, N., Strauss, R.D.: 2021, On the turbulent reduction of drifts for solar energetic particles. *Astrophys. J.* **922**, 200. DOI. ADS.

VanderPlas, J.T.: 2018, Understanding the Lomb–Scargle periodogram. *Astrophys. J. Suppl. Ser.* **236**, 16. DOI.

Whitman, K., Egeland, R., Richardson, I.G., Allison, C., Quinn, P., Barzilla, J., Kitiashvili, I., Sadykov, V., Bain, H.M., Dierckxsens, M., Mays, M.L., Tadesse, T., Lee, K.T., Semones, E., Luhmann, J.G., Núñez, M., White, S.M., Kahler, S.W., Ling, A.G., Smart, D.F., Shea, M.A., Tenishev, V., Boubrahimi, S.F., Aydin, B., Martens, P., Angryk, R., Marsh, M.S., Dalla, S., Crosby, N., Schwadron, N.A., Kozarev, K., Gorby, M., Young, M.A., Laurenza, M., Cliver, E.W., Alberti, T., Stumpo, M., Benella, S., Papaioannou, A., Anastasiadis, A., Sandberg, I., Georgoulis, M.K., Ji, A., Kempton, D., Pandey, C., Li, G., Hu, J., Zank, G.P., Lavasa, E., Giannopoulos, G., Falconer, D., Kadadi, Y., Fernandes, I., Dayeh, M.A., Muñoz-Jaramillo, A., Chatterjee, S., Moreland, K.D., Sokolov, I.V., Roussev, I.I., Taktakishvili, A., Effenberger, F., Gombosi, T., Huang, Z., Zhao, L., Wijsen, N., Aran, A., Poedts, S., Kouloumvakos, A., Paassilta, M., Vainio, R., Belov, A., Eroshenko, E.A., Abunina, M.A., Abunin, A.A., Balch, C.C., Malandraki, O., Karavolos, M., Heber, B., Labrenz, J., Kühl, P., Kosovichev, A.G., Oria, V., Nita, G.M., Illarionov, E., O'Keefe, P.M., Jiang, Y., Fereira, S.H., Ali, A., Paouris, E., Aminalragia-Giamini, S., Jiggens, P., Jin, M., Lee, C.O., Palmerio, E., Bruno, A., Kasapis, S., Wang, X., Chen, Y., Sanahuja, B., Lario, D., Jacobs, C., Strauss, D.T., Steyn, R., van den Berg, J., Swalwell, B., Waterfall, C., Nedal, M., Miteva, R., Dechev, M., Zucca, P., Engell, A., Maze, B., Farmer, H., Kerber, T., Barnett, B., Loomis, J., Grey, N., Thompson, B.J., Linker, J.A., Caplan, R.M., Downs, C., Török, T., Lionello, R., Titov, V., Zhang, M., Hosseinzadeh, P.: 2023, Review of solar energetic particle prediction models. *Adv. Space Res.* **72**, 5161. DOI. ADS.

Zank, G.P., Matthaeus, W.H., Smith, C.W.: 1996, Evolution of turbulent magnetic fluctuation power with heliocentric distance. *J. Geophys. Res.* **101**, 17093. DOI.
Zhao, L.-L., Adhikari, L., Zank, G., Hu, Q., Feng, X.: 2018, Influence of the solar cycle on turbulence properties and cosmic-ray diffusion. *Astrophys. J.* **856**, 94.

Publisher's Note Springer Nature remains neutral with regard to jurisdictional claims in published maps and institutional affiliations.